
Context-Dependent Manifold Learning: A Neuromodulated Constrained Autoencoder Approach

Jérôme Adriaens¹ Guillaume Drion¹ Pierre Sacré¹

Abstract

Constrained autoencoders (cAE) provide a successful path towards interpretable dimensionality reduction by enforcing geometric structure on latent spaces. However, standard cAEs cannot adapt to varying physical parameters or environmental conditions without conflating these contextual shifts with the primary input. To address this, we integrated a neuromodulatory mechanism into the cAE framework to allow for context-dependent manifold learning. This paper introduces the Neuromodulated Constrained Autoencoder (NcAE), which adaptively parameterizes geometric constraints via gain and bias tuning conditioned on static contextual information. Experimental results on dynamical systems show that the NcAE accurately captures how manifold geometry varies across different regimes while maintaining rigorous projection properties. These results demonstrate that neuromodulation effectively decouples global contextual parameters from local manifold representations. This architecture provides a foundation for developing more flexible, physics-informed representations in systems subject to (non-stationary) environmental constraints.

1. Introduction

Dimensionality reduction is a cornerstone of modern representation learning, enabling the extraction of tractable structures from high-dimensional data. While foundational techniques like Principal Component Analysis (PCA) provide a rigorous mathematical basis for linear subspaces, nonlinear alternatives, such as AutoEncoders (AEs) (Wang et al., 2016) and manifold learning techniques (e.g., t-SNE (van der Maaten & Hinton, 2008), Isomap (Tenenbaum et al., 2000), Kernel PCA (Schölkopf et al., 1997)), offer the

¹Neuroengineering Lab, Department of Electrical Engineering and Computer Science, University of Liège, Allée de la Découverte 11, Belgium. Correspondence to: Jérôme Adriaens <jadriaens@uliege.be>, Pierre Sacré <p.sacre@uliege.be>.

expressive power necessary to capture complex, nonlinear geometries.

Current nonlinear approaches often treat data as if it were drawn from a single, static distribution. However, in physical systems, the underlying manifold geometry is frequently governed by external parameters, such as varying Reynolds numbers in fluid dynamics or changing physical constants in robotics. Standard strategies typically address this by augmenting the input vector, but this often fails to preserve the intrinsic geometric structure of the state space across different regimes because the latent space becomes entangled with external parameters. Therefore, there is a need for a framework that can adapt to varying environmental conditions while maintaining rigorous geometric constraints.

To address this, we developed the Neuromodulated Constrained Autoencoder (NcAE), a framework designed for context-dependent manifold learning. We integrated a neuromodulatory mechanism (Vecoven et al., 2020) into the Constrained Autoencoder (cAE) (Otto et al., 2023) to adaptively tune network activation functions based on a static context vector. Unlike traditional conditional AEs that concatenate context at the input (Al Machot et al., 2022), our approach parameterizes the projection itself, allowing the model to learn a family of context-specific manifolds while maintaining rigorous geometric constraints. We investigated the effectiveness of this architecture on two dynamical systems: a 16-degree-of-freedom (DoF) pendulum (Friedl et al., 2025) and the Lorenz96 system (Lorenz, 1995).

This paper is organized as follows. Section 2 outlines the mathematical preliminaries for cAEs and the geometric requirements for projection operators. Section 3 details the NcAE architecture, including its shared embedding and context-dependent manifold transformations. Section 4 evaluates performance against baseline models across two dynamical systems. Finally, Section 5 discusses implications for reduced-order modeling and system identification, followed by concluding remarks in Section 6.

2. Background and Preliminaries

This section defines the mathematical framework for standard AEs and cAEs, and discusses the geometric constraints

required to transform them into formal projection operators.

2.1. Autoencoders as Nonlinear Mappings

An AE seeks to find a low-dimensional representation of a (high-dimensional) dataset $\mathcal{X} \subset \mathbb{R}^n$ by utilizing an encoder $\rho : \mathbb{R}^n \rightarrow \mathbb{R}^m$ and a decoder $\varphi : \mathbb{R}^m \rightarrow \mathbb{R}^n$, where $m \ll n$. The composition $P = \varphi \circ \rho$ defines a reconstruction mapping. While the bottleneck layers capture a compressed latent state $z \in \mathbb{R}^m$, standard AE formulations do not guarantee that P functions as a formal projection operator.

Most traditional models lack *idempotency* ($P \circ P = P$), meaning they fail to uniquely map high-dimensional states to their manifold representations. This deficiency causes representational drift and compromises physical consistency in the latent space. Furthermore, the absence of explicit geometric constraints often results in non-smooth manifold representations, which complicates the gradient computation necessary for physics-based tasks (Lee & Carlberg, 2019).

2.2. Constrained Autoencoders

To resolve the idempotency issue, the cAE enforces a critical geometric property: the composition of its encoder and decoder functions forms an idempotent projection operator (Otto et al., 2023). Mathematically, the cAE ensures that $\rho \circ \varphi = \text{id}_{\mathbb{R}^m}$. This equality makes making $P = \varphi \circ \rho$ a smooth, idempotent mapping, which guarantees that the learned manifold $\hat{\mathcal{M}} = \text{Range}(P)$ is a smooth embedded submanifold of the data space (Michor, 2008).

To implement this property in a neural network, the architecture constructs the encoder $\rho = \rho^{(1)} \circ \dots \circ \rho^{(L)}$ and the decoder $\varphi = \varphi^{(L)} \circ \dots \circ \varphi^{(1)}$ from pairwise layers (l). Each layer pair employs biorthogonal weight matrices Ψ_l and Φ_l , and smooth, mutually inverse activation functions (σ_-, σ_+):

$$\begin{aligned} \rho^{(l)}(\mathbf{x}^{(l)}) &= \sigma_- \left(\Psi_l^T (\mathbf{x}^{(l)} - \mathbf{b}_l) \right), \\ \varphi^{(l)}(\mathbf{z}^{(l-1)}) &= \Phi_l \sigma_+ \left(\mathbf{z}^{(l-1)} \right) + \mathbf{b}_l. \end{aligned}$$

This construction inherently satisfies the constraint $\Psi_l^T \Phi_l = \mathbf{I}$. We enforce this biorthogonality constraint during training via Riemannian optimization on the biorthogonal manifold using the `geoopt` library (Friedl et al., 2025). More details about the cAE can be found in Section A.

This approach ensures the learned manifold respects the underlying differential structure of the data, providing a stable foundation for the neuromodulation introduced in the next section.

3. Neuromodulated Constrained Autoencoder

This section describes our neuromodulated cAE (NcAE) by first defining the role of neuromodulation in context-dependent adaptation, then explaining the shared embedding used for scalability, and finally detailing the layer-specific parameters that govern the manifold transformations—see Figure 1 for a visual overview. This architecture enables the network to learn a family of manifolds parameterized by an external context vector \mathbf{c} while strictly maintaining the idempotency property required for physical consistency.

3.1. Neuromodulation Mechanism

To achieve the representation flexibility observed in biological systems, we introduce a neuromodulatory mechanism based on the work of Vecoven et al. (2020), which dynamically tunes the autoencoder properties. In nature, neuromodulation is a fundamental process that allows nervous systems to adapt to varying environments by adjusting the response characteristics of neurons and networks (Bargmann & Marder, 2013). By adopting this principle, we utilize a parameter-efficient hyper-network that conditions the primary network on an exogenous context vector \mathbf{c} .

Technically, we achieve this by setting the static parameters of the activation function of the cAE as neuromodulation targets of our method. We will write the context-dependent activation functions as $\sigma_{\pm}(\cdot; \boldsymbol{\alpha}^{(l)})$ and the context-dependent biases $\mathbf{b}^{(l)}$. By design, this parameterization is restricted such that the fundamental geometric properties of the cAE are maintained across all contextual shifts. These layer-specific parameters, $\boldsymbol{\alpha}^{(l)}$ and $\mathbf{b}^{(l)}$, are generated through a two-step process driven by a context vector \mathbf{c} .

3.2. Shared Neuromodulation Embedding

To ensure the scalability of the neuromodulatory mechanism, we employ a hierarchical approach to parameter generation that minimizes the total parameter count. Instead of mapping the context vector \mathbf{c} directly to high-dimensional layer parameters, we first project \mathbf{c} through a shared fully connected network to a lower-dimensional latent embedding $\mathbf{s} \in \mathbb{R}^d$. This shared embedding serves as a global neuromodulatory signal. This architectural bottleneck acts as a form of regularization; it prevents the model from overfitting to specific context values and ensures that the modulation remains computationally efficient across all network layers.

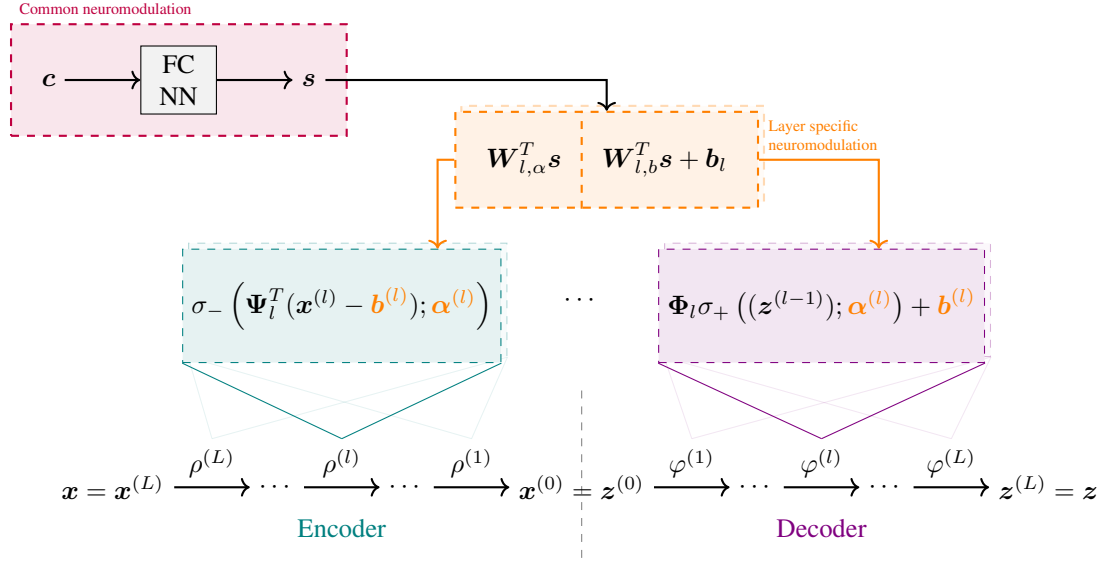


Figure 1. Neuromodulation dynamically reconfigures the autoencoder manifold by parameterizing activation functions and biases based on external context. This schematic illustrates the integration of the context vector \mathbf{c} , which is processed by a fully connected MLP to generate the modulation signal \mathbf{s} . This signal is then multiplied by a layer-specific weight matrix $\mathbf{W}_{l,\alpha}$ to compute the activation parameters $\alpha^{(l)}$. Simultaneously, \mathbf{s} passes through a linear layer defined by parameters $\mathbf{W}_{l,b}$ and \mathbf{b}_l to determine the layer-wise bias $\mathbf{b}^{(l)}$. Together, these components allow the model to adapt its internal transformations to the specific requirements of the provided context.

3.3. Layer-Specific Neuromodulation

For each layer pair l , this signal \mathbf{s} generates $\alpha^{(l)}$ and $\mathbf{b}^{(l)}$ according to

$$\begin{aligned}\alpha^{(l)} &= g(\mathbf{W}_{l,\alpha}^T \mathbf{s}) \\ \mathbf{b}^{(l)} &= \mathbf{W}_{l,b}^T \mathbf{s} + \mathbf{b}_l,\end{aligned}$$

where $\mathbf{W}_{l,\alpha}^T$, $\mathbf{W}_{l,b}^T$, and \mathbf{b}_l represent trainable layer-specific weights. The function g is a saturating transformation that constrains the α values within the valid range for the inverse activation functions (σ_- , σ_+) as explained in detail in Section B. By modulating these parameters, the NcAE flexibly adjusts its nonlinear transformations to suit the given context without violating the biorthogonality constraints of the underlying manifold. Figure 1 illustrates how the context vector \mathbf{c} influences these activation functions. More details can be found in Appendix B.

4. Experiments

This section assesses the performance of the NcAE across two distinct dynamical systems by comparing it against two baseline architectures: a context-free cAE and a standard Context-cAE. We first describe these architectural configurations and the common evaluation protocol, then present a quantitative analysis of reconstruction fidelity and latent space organization for each dynamical system.

To isolate the impact of the neuromodulatory mechanism, we compare three distinct architectures:

- *cAE*: A baseline constrained autoencoder that ignores contextual inputs, serving as a lower bound for representational accuracy across varying regimes.
- *Context-cAE*: A standard conditional architecture where the context vector \mathbf{c} is concatenated to the input \mathbf{x} . This model represents the conventional strategy of treating context as an additional input feature.
- *NcAE*: Our proposed architecture, which utilizes contextual information to drive coordinate transformations via the hierarchical neuromodulation mechanism described in Section 3.1.

This comparison aims to demonstrate that parameterizing the projection operator itself, rather than augmenting the input vector, not only preserves the intrinsic geometric structure of the state-space, but also enhances the fidelity of the dimensionality reduction. All models were trained using the hyperparameters detailed in Section C. The following subsections investigate how each architecture adapts to unseen test sets and characterize the resulting latent manifold organization.

4.1. 16-DoF Pendulum

This section assesses the NcAE ability to adapt to varying morphologies of a 16-degree-of-freedom (DoF) pendulum by comparing its performance across a standard (context-independent) configuration and a context-dependent coupling configuration. In the standard experiment, we ex-

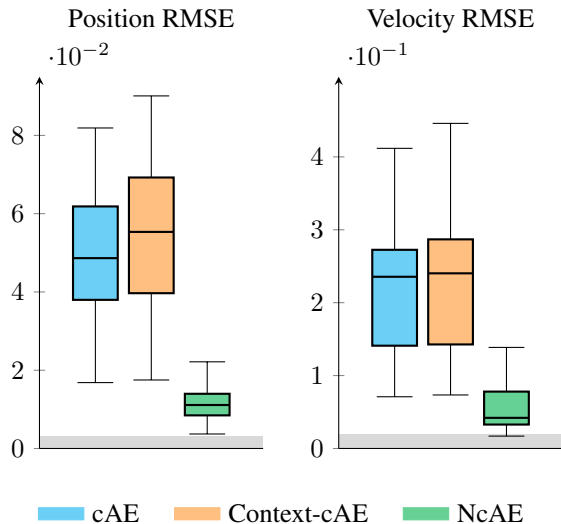


Figure 2. The NcAE significantly outperforms standard and conditional autoencoders, especially in reconstructing the underlying system dynamics under context-dependent coupling. This boxplot compares the root mean square error (RMSE) distribution across 256 test trajectories for three architectures. The shaded grey region indicates the baseline performance range observed in the *Standard pendulum* experiment where context does not influence coupling. The *left* panel shows the reconstruction error for the pendulum DoFs, while the *right* panel displays the error for their first-order derivatives. The results demonstrate that the NcAE ability to modulate its internal representation leads to a more accurate capture of both the state and its temporal evolution compared to simple context concatenation.

tended the setup from Friedl et al. (2025) by sampling the lengths of the first four links uniformly from $[0.35, 0.65]$ m while keeping the remaining 12 DoFs constant. In the context-dependent experiment, we modified the system so that the lengths and joint angles of the first 4 DoFs govern the coupling of the subsequent 12 DoFs. Full specifications for these coupling functions are provided in Section C.

4.1.1. RECONSTRUCTION RESULTS

The NcAE achieves a four-fold reduction in the reconstruction error over baseline methods when the system dynamics depend on morphological context. In the context-dependent experiment, the NcAE substantially outperformed both the baseline cAE and the Context-cAE, reducing the median root mean square error (RMSE) by approximately 75% for both position and velocity (Figure 2). Notably, the standard concatenation approach (Context-cAE) failed to provide meaningful improvement over the context-agnostic baseline. This result indicates that providing context as an input feature is insufficient for capturing shifting physical manifolds; instead, the NcAE successfully leverages neuromodulation to adapt the internal coordinate transformations to varying state relationships.

In contrast, all architectures exhibit comparable performance when the underlying manifold lacks contextual variability. In the standard pendulum experiment characterized by context-independent coupling, the error distributions for all three models remained similar. This outcome aligns with theoretical expectations: without morphological coupling, the specialized modulation of the NcAE is not required. The shaded grey region in Figure 2 represents this baseline limit for reconstruction accuracy on a static manifold.

4.1.2. LATENT ANALYSIS

Neuromodulation enables the latent space to reconfigure its geometry dynamically to accommodate physical constraints (variations in link lengths). As shown in Figure 3, the latent trajectories of the NcAE (right) exhibit clear translations and nonlinear deformations as the link lengths vary. Conversely, the representations for the cAE and Context-cAE (left and middle) remain largely invariant to morphological changes, explaining their inability to resolve the shifting physical coupling. This confirms that the neuromodulatory mechanism actively warps the manifold geometry in response to the context.

Beyond adaptation, the NcAE promotes a more efficient and balanced utilization of the latent capacity. While baseline models exhibit highly imbalanced axis scaling—with ranges for z_1 and z_2 differing by an order of magnitude—the NcAE demonstrates homogeneous scaling. This balanced representation allows the model to capture complex, context-dependent state relationships that a static projection cannot resolve, leading to the superior fidelity observed in the reconstruction tasks.

4.2. Lorenz96 Single-Scale Model

This section assesses the NcAE ability to capture state relationships that emerge intrinsically from physical dynamics by investigating the Lorenz96 system. Unlike the previous experiment, which utilized an explicitly imposed coupling function, the Lorenz96 system features complex, non-linear dynamics where the state-space topology is governed by an external forcing constant F . We evaluate how neuromodulation tracks these shifting manifolds across a critical bifurcation point.

The forcing constant F determines the system qualitative behavior, ranging from stable limit cycles to fully developed chaos. We focus on the range $F \in [3.133, 3.193]$, which contains a bifurcation at $F \approx 3.163$ where the attractor topology fundamentally changes. By generating trajectories from basins that lose stability beyond this threshold, we create a scenario where the relationship between state variables depends critically on F . This parameter serves as the contextual signal for three distinct experimental setups: *Standard Lorenz96a* (pre-bifurcation), *Standard Lorenz96b*

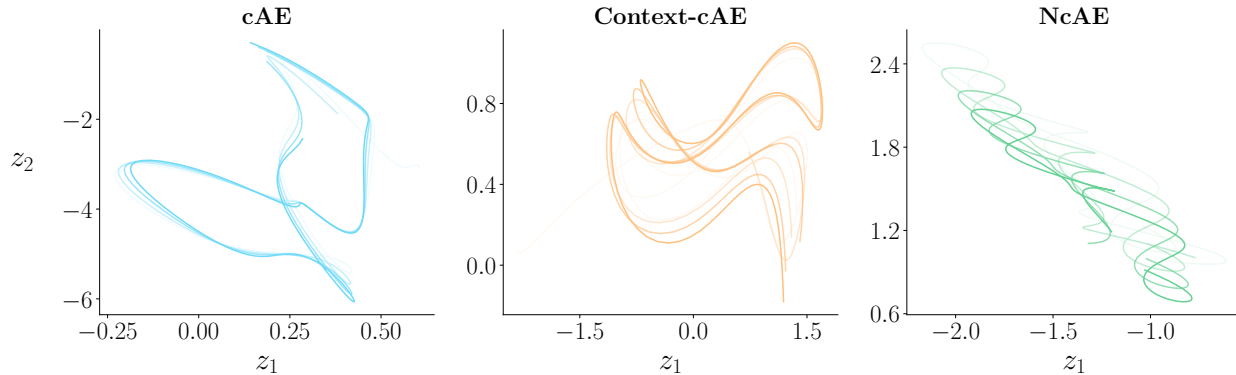


Figure 3. The NcAE exhibits a highly structured and continuous adaptation of its latent geometry in response to varying physical parameters. This figure visualizes latent trajectories for dimensions z_1 and z_2 across a range of configurations where all link lengths are held equal. The transparency gradient represents the transition from 0.35m (most transparent) to 0.65m (least transparent). While standard architectures often collapse or struggle to organize context-dependent data, the NcAE successfully partitions the latent space, demonstrating that the neuromodulation mechanism internalizes the relationship between the physical context (link lengths) and the resulting system manifold.

(post-bifurcation), and *Context Lorenz96* (full range).

4.2.1. RECONSTRUCTION RESULTS

The NcAE provides superior reconstruction fidelity by effectively disentangling state dynamics from global forcing pressures. As illustrated in Figure 4, the NcAE reduces the median state reconstruction error by at least 75% compared to both the baseline cAE and the Context-cAE. The performance gap is most pronounced in the reconstruction of the first-order derivatives, where the maximum error for the NcAE is nearly twofold smaller than the minimum error of the competing methods. Furthermore, the Hovmöller diagrams in Figure 5 confirm that the NcAE consistently produces fewer local errors across the spatial domain than the baseline architectures.

Adaptive scaling of activation functions allows the NcAE to represent varying derivative profiles that static manifolds cannot capture. This performance gain stems from the neuromodulatory α parameter, which adjusts the slope of the activation functions. By dynamically tuning these nonlinearities, the NcAE scales its internal derivatives to match the specific physical regime. In contrast, the standard concatenation approach in the Context-cAE remains unable to provide a meaningful improvement, suggesting that treating F as an input feature fails to resolve the underlying manifold deformation.

4.2.2. LATENT ANALYSIS

Neuromodulation promotes a more regularized and adaptive latent organization compared to standard concatenation. In matched-context settings, the NcAE exhibits subtle, context-

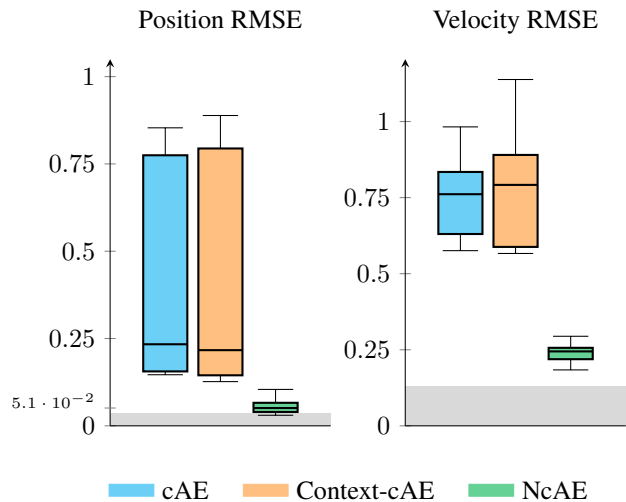


Figure 4. The NcAE maintains high-fidelity reconstruction across critical bifurcations, where baseline architectures fail to adapt to changing system dynamics. These boxplots illustrate the distribution of the RMSE for both state reconstruction and first-order derivatives across test trajectories spanning the full range of forcing parameters F . The shaded grey region represents the performance benchmarks from the *Standard Lorenz 96a* and *Standard Lorenz 96b* experiments; in these stable regimes, all architectures perform similarly well, with error magnitudes that are negligible relative to the scale of the illustrated plots. However, in the context-dependent case, the NcAE neuromodulation allows it to resolve the shifting manifold structure that causes significant error spikes in the non-modulated models.

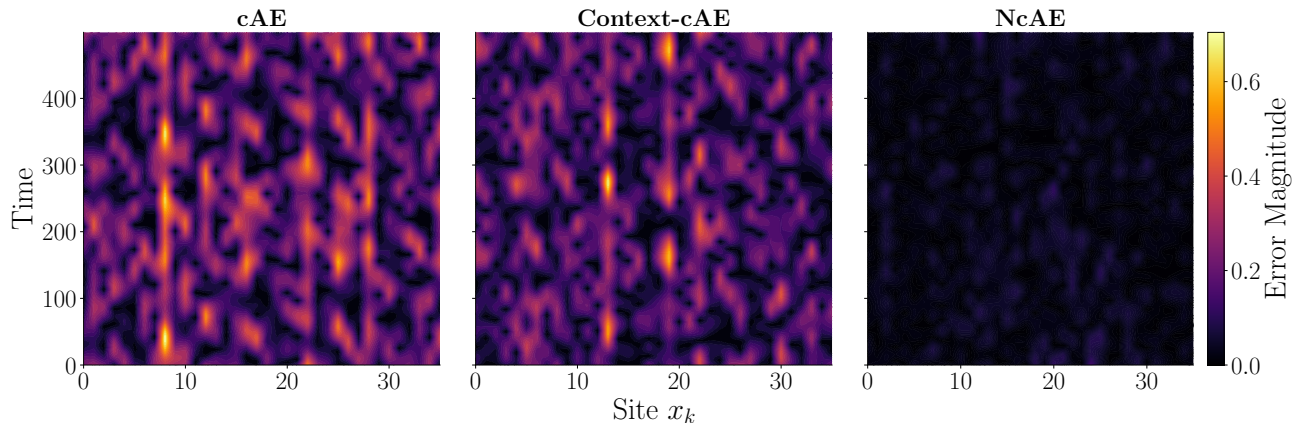


Figure 5. The NcAE provides a context-specific manifold alignment that minimizes systematic spatio-temporal reconstruction errors. This figure displays Hovmöller diagrams of the absolute error between the ground truth and the reconstruction for a trajectory at $F = 3.133$. By utilizing a neuromodulation signal tailored to this specific forcing parameter, the NcAE avoids the structured error patterns seen in architectures that lack the flexibility to adapt their internal transformations to the specific regime.

dependent modifications to its latent orbits that suggest an adaptive projection (Figure 6). While the cAE and Context-cAE produce highly inhomogeneous latent velocities and imbalanced axis ranges, the NcAE maintains consistent velocity norms and homogeneous axis scaling. This balanced utilization of latent capacity suggests that neuromodulation inherently regularizes the manifold, as previously observed in the pendulum study (Section 4.1.2).

The NcAE successfully internalizes the contextual signal as a driver for coordinate transformation, whereas concatenation remains static. Mismatched-context evaluations reveal that while both the Context-cAE and NcAE capture fundamental state relationships via their primary weights, only the NcAE remains sensitive to the modulating input (Figure 7). When processing a fixed trajectory while sweeping F , the Context-cAE maintains an identical latent representation, indicating that the concatenated context is effectively ignored. In contrast, the NcAE significantly reshapes the latent projection as F varies, demonstrating its ability to use context to actively parameterize the coordinate mapping.

5. Discussion

The NcAE extends the rigorous projection properties of constrained autoencoders (Otto et al., 2023) to multi-context environments, providing a stable foundation for Reduced Order Modeling (ROM) across varying physical regimes. While our experiments utilized physical parameters as context, the architecture remains inherently general; the vector c can represent any exogenous signal. Unlike other learned conditioning methods such as FiLM (Perez et al., 2017) or Attention (Vaswani et al., 2017)—which are typically applied to unconstrained models—the NcAE preserves the manifold differential structure by parameterizing the pro-

jection operator itself. This mathematical consistency is a prerequisite for downstream tasks that require stable gradients and idempotent mappings.

The success of the NcAE in adapting to bifurcating dynamics suggests significant potential for integration with latent-space system identification. By providing a “context-aware” coordinate system, the NcAE facilitates the discovery of universal governing equations via frameworks such as SINDy (Brunton et al., 2016), Hamiltonian Neural Networks (Greydanus et al., 2019), or Neural ODEs (Chen et al., 2019). Such coupling would enable the identification of unified dynamical models that generalize across entire families of physical systems, eliminating the need for regime-specific retraining and providing a more robust path toward automated scientific discovery.

6. Conclusion and Future Work

This paper has presented the NcAE, a framework for context-dependent manifold learning that maintains the rigorous projection properties necessary for physical consistency. Our results on high-dimensional pendulums and the Lorenz96 system demonstrate that a shared neuromodulatory embedding effectively tracks structural transitions in dynamics—such as bifurcations—without the parameter explosion typical of standard hyper-networks. We conclude that internalizing contextual signals as drivers for coordinate transformations, rather than as simple input features, is essential for high-fidelity representation of parameter-dependent manifolds.

Future research will investigate the integration of this framework with data-driven system identification to discover universal governing equations. By providing a stable yet flexible coordinate system that respects the underlying geometry of the state-space, the NcAE enables the development of

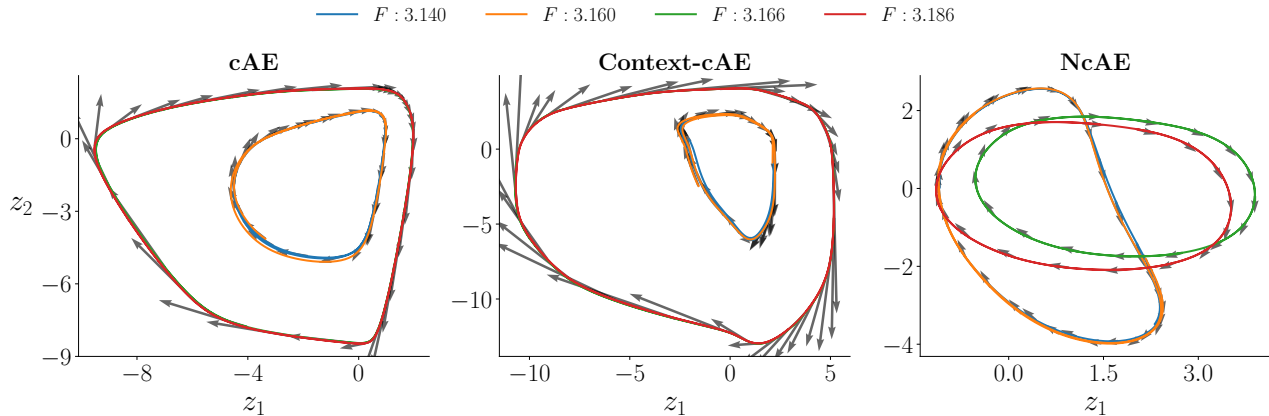


Figure 6. The NcAE maintains a balanced and regularized latent manifold across forcing regimes, avoiding the distorted velocities and imbalanced scaling seen in standard architectures. This figure visualizes the latent trajectories for various forcing parameters F across the three architectures, with arrows representing the projected first-order derivatives. While the cAE and Context-cAE exhibit highly inhomogeneous latent velocities and poorly scaled axes, the NcAE produces a more uniform and consistent representation. This suggests that the context-specific modulation of activation functions and biases acts as an implicit regularizer, ensuring a more efficient and geometrically stable utilization of the latent capacity regardless of the underlying system dynamics.

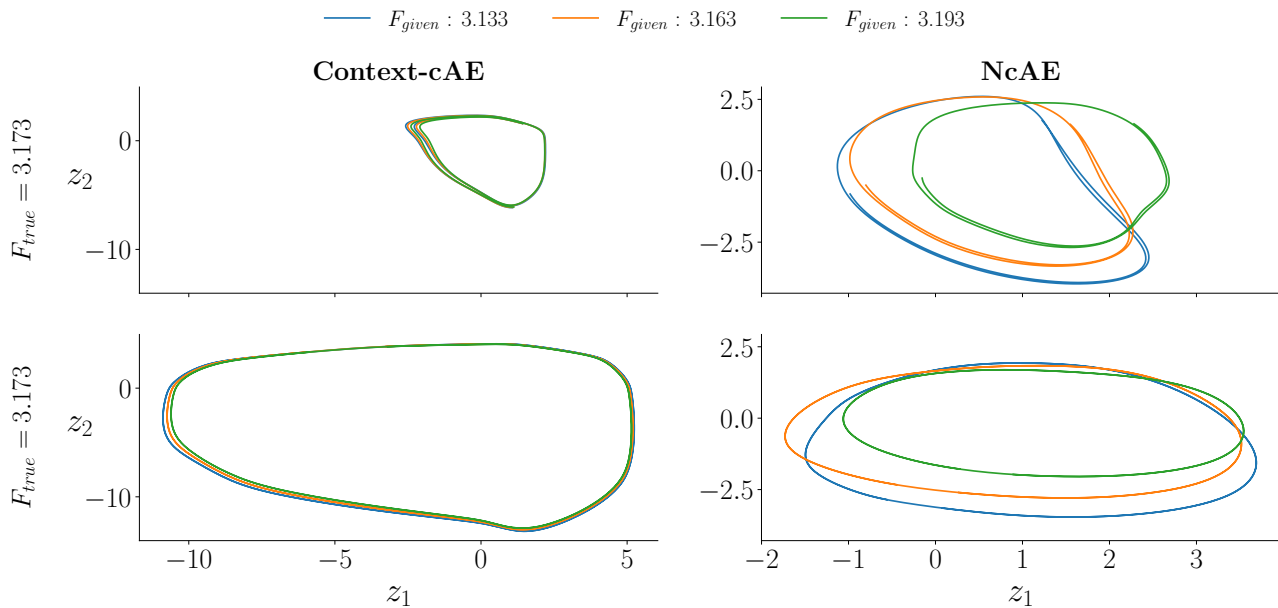


Figure 7. The NcAE possesses a context-aware latent geometry that actively reshapes its representation, whereas the Context-cAE remains rigid and non-adaptive. This figure evaluates the model sensitivity by encoding a fixed trajectory (generated at a constant F_{true}) while varying the provided context F_{given} . In the left column, the Context-cAE produces nearly identical latent orbits regardless of the provided context, demonstrating that simple concatenation fails to induce structural adaptation. In contrast, the right column shows the NcAE undergoing significant representational drift; the model neuromodulated parameters actively reconfigure the latent manifold to align with the "expected" dynamics of the provided context, even when it conflicts with the true underlying data.

reduced-order models that remain valid across diverse environmental conditions and critical physical transitions. These perspectives suggest that neuromodulation is a powerful tool for bridging the gap between rigid geometric constraints and the inherent variability of real-world physical systems.

Acknowledgements

This work was supported by the Belgian Government through the Federal Public Service Policy and Support. The present research benefited from computational resources made available on Lucia, the Tier-1 supercomputer of the Walloon Region, infrastructure funded by the Walloon Region under the grant agreement n°1910247.

References

- Al Machot, F., Ullah, M., and Ullah, H. HFM: A Hybrid Feature Model Based on Conditional Auto Encoders for Zero-Shot Learning. *Journal of Imaging*, 8(6):171, June 2022. ISSN 2313-433X. doi: 10.3390/jimaging8060171.
- Bargmann, C. I. and Marder, E. From the connectome to brain function. *Nature Methods*, 10(6):483–490, June 2013. ISSN 1548-7105. doi: 10.1038/nmeth.2451.
- Brunton, S. L., Proctor, J. L., and Kutz, J. N. Discovering governing equations from data: Sparse identification of nonlinear dynamical systems. *Proceedings of the National Academy of Sciences*, 113(15):3932–3937, April 2016. ISSN 0027-8424, 1091-6490. doi: 10.1073/pnas.1517384113.
- Chen, R. T. Q., Rubanova, Y., Bettencourt, J., and Duvenaud, D. Neural Ordinary Differential Equations, December 2019.
- Friedl, K., Jaquier, N., Lundell, J., Asfour, T., and Kragic, D. A riemannian framework for learning reduced-order lagrangian dynamics. In *Intl. Conf. on Learning Representations (ICLR)*, 2025.
- Glashoff, K. and Bronstein, M. M. Optimization on the biorthogonal manifold, September 2016.
- Greydanus, S., Dzamba, M., and Yosinski, J. Hamiltonian Neural Networks, September 2019.
- Kochurov, M., Karimov, R., and Kozlukov, S. Geoopt: Riemannian optimization in pytorch, 2020.
- Lee, K. and Carlberg, K. Model reduction of dynamical systems on nonlinear manifolds using deep convolutional autoencoders, June 2019.
- Lorenz, E. *Predictability: A Problem Partly Solved*. PhD thesis, ECMWF, Shinfield Park, Reading, 1995.
- Michor, P. *Topics in Differential Geometry*, volume 93 of *Graduate Studies in Mathematics*. American Mathematical Society, Providence, Rhode Island, July 2008. ISBN 978-0-8218-2003-2 978-1-4704-1161-9. doi: 10.1090/gsm/093.
- Otto, S. E., Macchio, G. R., and Rowley, C. W. Learning Nonlinear Projections for Reduced-Order Modeling of Dynamical Systems using Constrained Autoencoders, September 2023.
- Perez, E., Strub, F., de Vries, H., Dumoulin, V., and Courville, A. FiLM: Visual Reasoning with a General Conditioning Layer, December 2017.
- Schölkopf, B., Smola, A., and Müller, K.-R. Kernel principal component analysis. In Gerstner, W., Germond, A., Hasler, M., and Nicoud, J.-D. (eds.), *Artificial Neural Networks — ICANN’97*, pp. 583–588, Berlin, Heidelberg, 1997. Springer. ISBN 978-3-540-69620-9. doi: 10.1007/BFb0020217.
- Tenenbaum, J. B., de Silva, V., and Langford, J. C. A global geometric framework for nonlinear dimensionality reduction. *Science*, 290(5500):2319–2323, December 2000. ISSN 0036-8075. doi: 10.1126/science.290.5500.2319.
- Todorov, E., Erez, T., and Tassa, Y. Mujoco: A physics engine for model-based control. In *2012 IEEE/RSJ International Conference on Intelligent Robots and Systems*, pp. 5026–5033. IEEE, 2012. doi: 10.1109/IROS.2012.6386109.
- van der Maaten, L. and Hinton, G. Visualizing Data using t-SNE. *Journal of Machine Learning Research*, 9(86): 2579–2605, 2008. ISSN 1533-7928.
- Vaswani, A., Shazeer, N., Parmar, N., Uszkoreit, J., Jones, L., Gomez, A. N., Kaiser, Ł., and Polosukhin, I. Attention is all you need. In Guyon, I., Luxburg, U. V., Bengio, S., Wallach, H., Fergus, R., Vishwanathan, S., and Garnett, R. (eds.), *Advances in Neural Information Processing Systems*, volume 30. Curran Associates, Inc., 2017.
- Vecoven, N., Ernst, D., Wehenkel, A., and Drion, G. Introducing neuromodulation in deep neural networks to learn adaptive behaviours. *PLOS ONE*, 15(1):e0227922, January 2020. ISSN 1932-6203. doi: 10.1371/journal.pone.0227922.
- Wang, Y., Yao, H., and Zhao, S. Auto-encoder based dimensionality reduction. *Neurocomputing*, 184:232–242, April 2016. ISSN 0925-2312. doi: 10.1016/j.neucom.2015.08.104.

A. Constrained autoencoder details

The constrained autoencoder was initially proposed by [Otto et al. \(2023\)](#). They impose that their autoencoder is a projection to leverage the autoencoder for projection-based reduced order modeling. The autoencoder is composed of an encoder ρ and a decoder φ such that the encoder maps the data space \mathcal{X} to a latent space \mathcal{Z} , and the decoder reconstructs the data from the latent space. By imposing $\rho \circ \varphi = \text{id}_{\mathcal{Z}}$, we ensure that $P = \varphi \circ \rho$ is a projection. In this case, P is smooth and idempotent, so $\mathcal{M} = \text{Range}(P)$ is a smooth embedded submanifold of \mathcal{X} ([Otto et al., 2023](#); [Michor, 2008](#)). The encoder ρ and decoder φ are defined as a composition of layers such that $\rho = \rho^{(1)} \circ \dots \circ \rho^{(L)}$ and $\varphi = \varphi^{(L)} \circ \dots \circ \varphi^{(1)}$, where $\rho^{(l)} : \mathbb{R}^{n_l} \rightarrow \mathbb{R}^{n_{l-1}}$ and $\varphi^{(l)} : \mathbb{R}^{n_{l-1}} \rightarrow \mathbb{R}^{n_l}$. Denoting d the latent space dimension and n the input space dimension, $d = n_0 \leq \dots \leq n_L = n$.

A.1. Biorthogonal layers

To ensure the geometric properties of the cAE, the encoder ρ and decoder φ are constructed with specific layer structures. Each layer transformation for the encoder and decoder can be expressed as:

$$\rho^{(l)}(\mathbf{x}^{(l)}) = \sigma_{-} \left(\Psi_l^T (\mathbf{x}^{(l)} - \mathbf{b}_l) \right) \quad \text{and} \quad \varphi^{(l)}(\mathbf{z}^{(l-1)}) = \Phi_l \sigma_{+} \left(\mathbf{z}^{(l-1)} \right) + \mathbf{b}_l, \quad (1)$$

where $\Psi_l \in \mathbb{R}^{(n_{l-1} \times n_l)}$ and $\Phi_l \in \mathbb{R}^{(n_l \times n_{l-1})}$ are the weight matrices for the encoder and decoder layers, respectively. The pair (σ_{-}, σ_{+}) consists of smooth activation functions that are inverses of one another, and \mathbf{b}_l are the bias vectors. Note that the biases \mathbf{b}_l are part of the targets parameters for our neuromodulation.

For each layer to satisfy the idempotent property $\rho^{(l)} \circ \varphi^{(l)} = \text{id}_{\mathbb{R}^{n_{l-1}}}$, a crucial condition must be met by the weight matrices:

$$\Psi_l^T \Phi_l = I_{\mathbb{R}^{n_{l-1}}}. \quad (2)$$

This defines Φ_l and Ψ_l as biorthogonal matrices ([Glashoff & Bronstein, 2016](#)). This condition can be enforced in several ways. The approach from [Otto et al. \(2023\)](#) involves an overparametrization of weight matrices followed by a projection map onto the biorthogonal manifold, though this introduces additional loss terms. Building upon this, [Friedl et al. \(2025\)](#) proposed an alternative: they ensure biorthogonality by using a specific geometric optimization framework, minimizing their loss function via Riemannian optimization directly on the biorthogonal manifold. Following their methodology, we adopt this geometric optimization approach for our training process, implemented using the Python package `geoopt` ([Kochurov et al., 2020](#)).

A.2. Activation functions

The activation functions used in the cAE are a crucial component, designed to be smooth and invertible, with the encoder and decoder utilizing inverse pairs (σ_{-}, σ_{+}) . These specific functions were first presented by [Otto et al. \(2023\)](#) as part of the cAE framework. They are derived from a particular form of hyperbola where the upper and lower branches are reflections of one another with respect to the axis $y = x$.

More formally, the expression for this inverse pair is:

$$\sigma_{\pm}(\mathbf{x}) = \frac{b\mathbf{x}}{a} \mp \frac{\sqrt{2}}{a \sin(\alpha)} \pm \frac{1}{a} \sqrt{\left(\frac{2\mathbf{x}}{\sin(\alpha) \cos(\alpha)} \mp \frac{\sqrt{2}}{\cos(\alpha)} \right)^2 + 2a},$$

where

$$a = \csc^2(\alpha) - \sec^2(\alpha), \quad b = \csc^2(\alpha) + \sec^2(\alpha), \quad \text{with } 0 < \alpha < \pi/4.$$

Notably, the parameter α in these equations is one of the targets for our neuromodulation, allowing the activation functions to adapt based on context (details in Section B). A visualization of these activation functions for different values of α is provided in Section A.2.

B. Neuromodulation details

Neuromodulation in biological neural systems refers to the process by which neuromodulators (such as dopamine or serotonin) modulate neuronal activity and synaptic properties, enabling adaptive responses. Unlike classical neurotransmission,

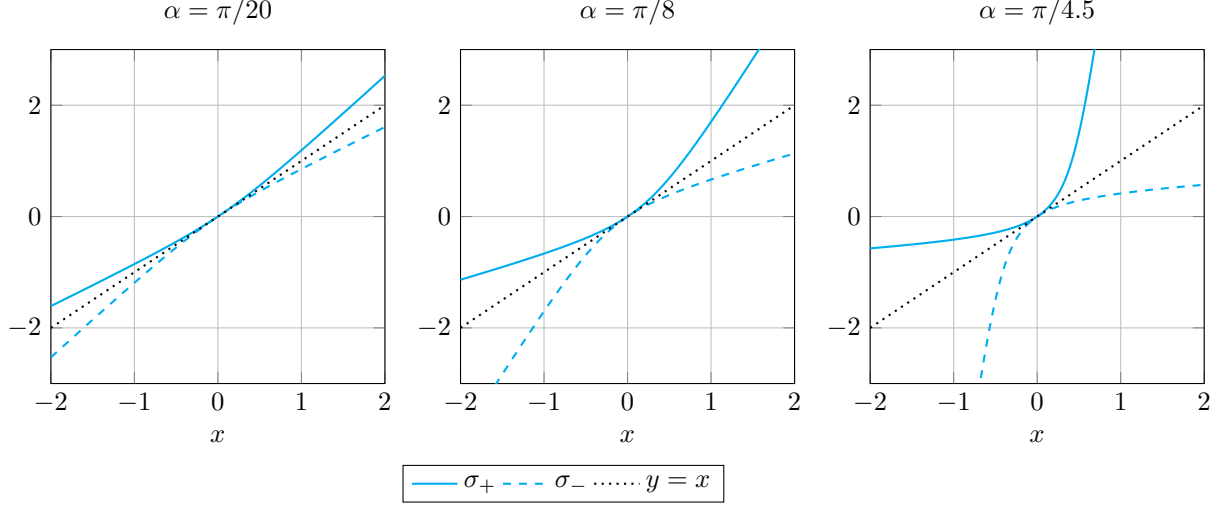


Figure 8. Activation functions σ_{\pm} for different values of α .

neuromodulation can act broadly across neural circuits, allowing the same network to produce different outputs depending on the neuromodulatory context (Bargmann & Marder, 2013). In artificial neural networks, this concept translates into dynamically adjusting network parameters based on contextual information, allowing the same network architecture to exhibit different behaviors depending on the input context. In our neuromodulated constrained autoencoder, we implement context-dependent activation functions where the activation parameters $\alpha^{(l)}$ and bias vectors $\mathbf{b}^{(l)}$ for a pair of layers l are modulated by a context vector \mathbf{c} .

Modulated activation functions The encoder and decoder layers in our method use context-dependent activation functions:

$$\rho^{(l)}(\mathbf{x}^{(l)}) = \sigma_{-} \left(\Psi_l^T(\mathbf{x}^{(l)} - \mathbf{b}^{(l)}); \alpha^{(l)} \right), \quad (3)$$

$$\varphi^{(l)}(\mathbf{z}^{(l-1)}) = \Phi_l \sigma_{+} \left(\mathbf{z}^{(l-1)}; \alpha^{(l)} \right) + \mathbf{b}^{(l)}, \quad (4)$$

where the parameter α from Section A.2 becomes variable and is specific to each input dimension, such that it writes now $\alpha^{(l)} \in \mathbb{R}^{n_l-1}$. In addition, the values $\alpha^{(l)}$ are constrained to lie within a specific range $[10^{-5}, \frac{\pi}{8}]$ which is more restrictive than the initial setting with the range $]0, \frac{\pi}{4}[$. The reason behind this can be shown in Figure 9 where we can see that for α values close to $\pi/4$, we have very steep slopes which can cause issues with training. Alternatively, the biases $\mathbf{b}^{(l)}$ are left unconstrained.

The neuromodulation process follows a two-stage mechanism:

Stage 1: Context processing The context vector $\mathbf{c} \in \mathbb{R}^{d_c}$ is first processed through a fully-connected neural network to generate a neuromodulation signal:

$$\mathbf{s} = f_{\text{nm}}(\mathbf{c}; \boldsymbol{\theta}), \quad (5)$$

where f_{nm} is a multilayer perceptron with parameters $\boldsymbol{\theta}$, and $\mathbf{s} \in \mathbb{R}^{d_s}$ is the resulting neuromodulation signal. We denote d_s and d_c as the dimensions of the neuromodulation signal and context vector, respectively.

Stage 2: Layer-specific modulation For each pair of layers l , the neuromodulation signal is transformed into intermediate layer-pair-specific activation parameters:

$$\bar{\alpha}^{(l)} = \mathbf{W}_{l,\alpha}^T \mathbf{s}, \quad (6)$$

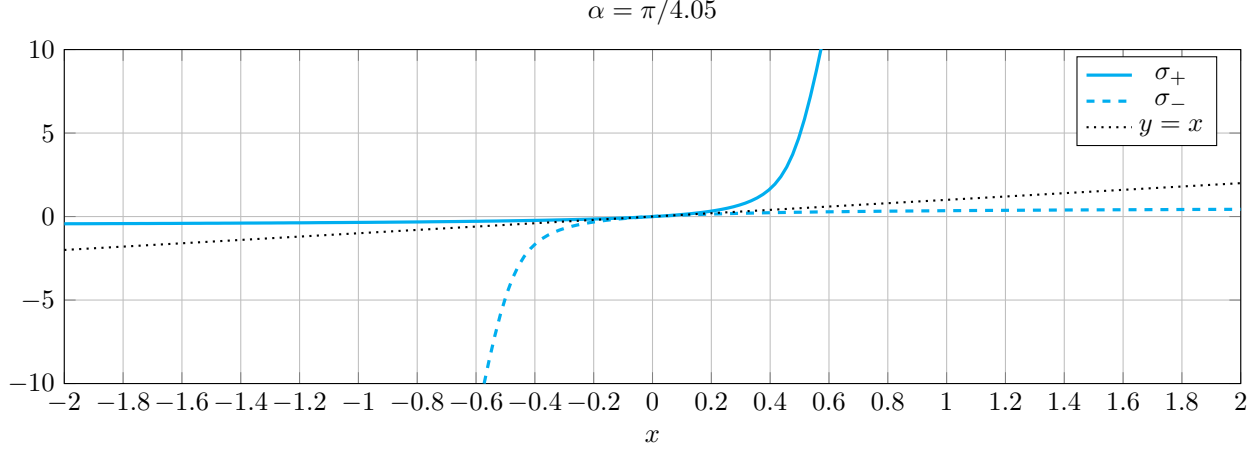


Figure 9. Activation functions σ_{\pm} for α near $\frac{\pi}{4}$.

where $\mathbf{W}_{l,\alpha} \in \mathbb{R}^{d_s \times n_l - 1}$ is a learnable transformation matrix specific to layer pair l . Then, to ensure that the activation parameters $\alpha^{(l)}$ lie within the desired range, we apply a scaled and shifted sigmoid function:

$$\alpha^{(l)} = (\alpha_{\max} - \alpha_{\min}) \cdot \text{SIGMOID}(\bar{\alpha}^{(l)}) + \alpha_{\min}, \quad (7)$$

$$\text{SIGMOID}(\mathbf{x}) = \frac{1}{1 + \exp(-\mathbf{x})} \quad (8)$$

where α_{\min} and α_{\max} are the minimum and maximum values for the activation parameters, respectively, and $\alpha^{(l)} \in \mathbb{R}^{n_l - 1}$ contains the parameters for the activation functions in that layer pair. The biases vector $\mathbf{b}^{(l)}$ is computed as

$$\mathbf{b}^{(l)} = \mathbf{W}_{l,b}^T \mathbf{s} + \mathbf{b}_l, \quad (9)$$

where $\mathbf{W}_{l,b}^T \in \mathbb{R}^{d_s \times n_l}$ and $\mathbf{b}_l \in \mathbb{R}^{n_l}$ are learnable parameters.

C. 16-DoF Pendulum Experimentations Details

The experimental setup consists of two main parts, both centered on a 16-DoF pendulum system. The first four pendulum links are modeled in *MuJoCo* (Todorov et al., 2012) as a capsule with a fixed radius of 0.05 m and a mass of 1.0 kg, while the other DoF come from the coupling with the first 4 joints. The context vector \mathbf{c} consists of the four link lengths (l_1 to l_4).

C.1. Standard coupling

In the first experiment, the initial 4 DoF (q_1 to q_4) correspond to the angles of the first four pendulum links. For each simulation, the lengths of these four links (l_1 to l_4) are randomly sampled from a uniform distribution in the range $[0.35, 0.65]$ m. The remaining 12 DoF (q_5 to q_{16}) are generated using nonlinear coupling functions that depend only on the first four angles q_1 to q_4 , as detailed in Table 1. This setup allows us to investigate how the different AEs capture the underlying manifold structure when the context (link lengths l_i) varies but does not directly affect the coupling.

C.2. Context-dependent coupling

The second experiment extends the first by introducing context-dependent coupling. Here, the nonlinear coupling functions for the last 12 DoF are modified to explicitly depend on both the angles (q_1 to q_4) and the corresponding link lengths (l_1 to l_4), as shown in Table 1. This creates a scenario where the context vector (link lengths) directly influences the relationships between the DoF, making the underlying manifold structure context-dependent. This experiment aims to show that relevant context information is crucial to learn the manifold structure effectively and that the NcAE can use this information to improve its performance.

Table 1. Coupling functions.

(a) Standard Coupling		(b) Context-dependent Coupling	
DoF	$f(q_1, q_2, q_3, q_4)$	DoF	$f(q_1, q_2, q_3, q_4, l_1, l_2, l_3, l_4)$
q_5	$q_3 - \cos(q_2)$	q_5	$q_3 - \cos(2l_2q_2)$
q_6	$q_1 + 0.1 \sin(q_2)$	q_6	$q_1 + 2l_1 0.1 \sin(2l_2q_2)$
q_7	$q_4 \cos(q_2)$	q_7	$q_4 \cos(2l_4q_2)$
q_8	$q_1 + q_3^2$	q_8	$q_1 + q_3^{2 \cdot 2l_3}$
q_9	$1.5 \sin(q_2)$	q_9	$2l_2 1.5 \sin(q_2)$
q_{10}	$-q_4q_1$	q_{10}	$-(l_4 + l_1)q_4q_1$
q_{11}	$\sin(q_1)$	q_{11}	$\sin(2l_1q_1)$
q_{12}	$0.4q_3q_4$	q_{12}	$2l_3 0.4q_3q_4$
q_{13}	$-0.9q_1 - q_2 + q_3 - 2q_4^2$	q_{13}	$-2l_1 0.9q_1 - q_2 + q_3 - 2q_4^{2 \cdot 2l_4}$
q_{14}	$-3 \sin(q_3)$	q_{14}	$-2l_3 3 \sin(q_3)$
q_{15}	$-2q_3^2$	q_{15}	$-2q_3^{2 \cdot 2l_3}$
q_{16}	$-0.9q_1^2$	q_{16}	$-0.9q_1^{2 \cdot 2l_1}$

C.3. Data collection

This section details the procedure for collecting data for our dataset. We begin by uniformly sampling the first four link lengths from the range $[0.35, 0.65]$ m. Each such pendulum configuration is then simulated in *MuJoCo* for 3s with a timestep of 1ms. For the training dataset, we collect 100 trajectories. For each sampled link length configuration, the initial configuration of the first four joints is uniformly sampled from $[0, 30]^\circ$. For the test dataset, we sample 256 distinct link length configurations by taking all possibilities from the set $\{0.35, 0.45, 0.55, 0.65\}^4$ m. For these test configurations, the initial angle for all joints is consistently set to 15° . This regular, systematic sampling for the test set is chosen to provide a comprehensive and unbiased evaluation of our model performance across a representative grid of contextual parameters, ensuring robust assessment of context-dependent behavior.

C.4. Architecture and training details

The hyperparameters used for the 3 architectures (cAE, Context-cAE and NcAE) are summarized in Table 2. The layers sizes n_l refer to the biorthogonal layer pairs within the encoder $\rho^{(l)} : \mathbb{R}^{n_l} \rightarrow \mathbb{R}^{n_{l-1}}$ and the decoder $\varphi^{(l)} : \mathbb{R}^{n_{l-1}} \rightarrow \mathbb{R}^{n_l}$. The loss used for optimizing the parameters of the different AEs is as follows

$$\mathcal{L}_{ae} = \frac{1}{N} \sum_{i=0}^N (\mathbf{x} - P(\mathbf{x}))^2 + (\dot{\mathbf{x}} - \nabla_{\mathbf{x}} P(\mathbf{x}) \cdot \dot{\mathbf{x}})^2$$

where N is the batch size, and $P(\mathbf{x}) = \varphi \circ \rho(\mathbf{x})$.

D. Lorenz96 Experimentations Details

The second set of experiments focuses on the Lorenz96 dynamical system (Lorenz, 1995), a high-dimensional model that exhibits complex nonlinear phenomena including limit cycles and chaos. The system consists of $N = 36$ variables governed by the following equations:

$$\dot{x}_k = (x_{k+1} - x_{k-2})x_{k-1} - x_k + F, \quad k = 1, \dots, N$$

with periodic boundary conditions $x_k = x_{k+N}$. In this setup, the context vector c is the scalar forcing constant F .

D.1. Standard regimes

To benchmark the architectures under context-independent conditions, we define two standard regimes:

- **Standard Lorenz96a:** F is sampled from a narrow range $[3.133, 3.163]$. In this regime, the system is characterized by the presence of two stable limit cycles.

Table 2. Hyperparameters for the 16-DoF Pendulum Experiment.

Hyperparameter	cAE	Context-cAE	NcAE
<i>Main Architecture</i>			
Layer Sizes (n_l)		[8, 16, 16, 16]	[8, 12, 14, 16]
Latent Dimension (d)		4	
Activation parameter α		$\pi/8$	N/A
<i>Contextual Mechanism</i>			
Mechanism	None	Concatenation	Neuromodulation
MLP Topology		N/A	[4, 4, 4]
MLP Activation		N/A	SiLU
Learning rate		N/A	$5 \cdot 10^{-3}$
Weight Decay		N/A	10^{-3}
<i>Optimization</i>			
Optimizer		Riemannian Adam (geoopt)	
Learning Rate		$5 \cdot 10^{-2}$	
Weight Decay		10^{-5}	
Epochs		5000	
Batch Size		4096	
Scheduler		ReduceLRonPlateau (Patience 200, Factor 0.9)	

- **Standard Lorenz96b:** F is sampled from the range [3.163,3.193]. This regime follows a critical bifurcation where one of the previously stable attractors becomes unstable.

In these cases, the forcing parameter F is provided to the models, but since the range is restricted to a single topological regime, the necessity for context-dependent manifold adaptation is minimized. Hovmöller diagrams in Figure 10 illustrate the two dynamical regimes. The system transitions from a traveling wave with a spatial frequency of 8 at $F = 3.133$ to a frequency of 7 at $F = 3.193$.

D.2. Context-dependent dynamics (Bifurcation)

The main experiment, *Context Lorenz96*, utilizes the full range $F \in [3.133, 3.193]$. Unlike the pendulum experiment, the “coupling” here is not an explicitly defined function but emerges from the integration of the ODEs. As F crosses the bifurcation point $F \approx 3.163$, the relationship between state variables x_k changes qualitatively. This experiment tests whether the NcAE can internalize these intrinsic shifts in the state-space manifold by modulating its internal transformations based on the value of F .

D.3. Data collection

The dataset is generated by integrating the Lorenz96 equations using a 4th-order Runge-Kutta method with a timestep of $\Delta t = 0.01$. For the training set, we generate 18 trajectories. For each trajectory, the forcing F is sampled uniformly from [3.133, 3.193]. The initial condition is set to $x_k(0) = F + \sin 8.05 \cdot \frac{2\pi k}{N}$ to ensure the states go to one attractor or the other depending on F . The ODEs are integrated for a transient period to ensure the state lies on an attractor. Each trajectory consists of 500 time points. For the test set, we systematically sample 10 values of F linearly spaced across the range [3.133, 3.193].

D.4. Architecture and training details

The hyperparameters used for the 3 architectures (cAE, Context-cAE and NcAE) are summarized in Table 3 and use the same loss \mathcal{L}_{ae} as defined in Section C.4. The latent size is set to $d = 2$, as the system dynamics in this regime are characterized by limit cycles which can be embedded in a 2D manifold.

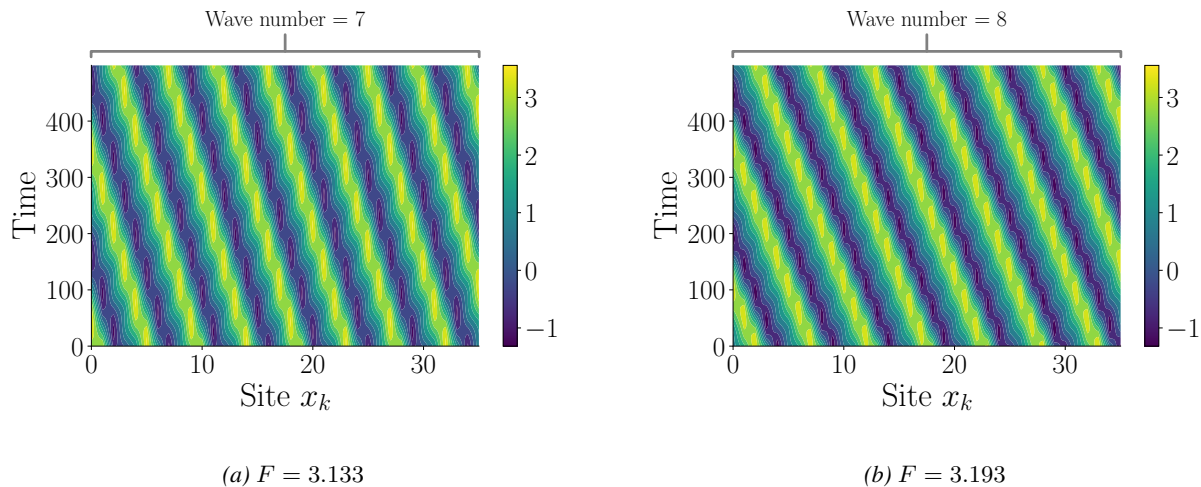


Figure 10. Hovmöller diagrams of the Lorenz96 system for values of F before and after the bifurcation.

Table 3. Hyperparameters for the Lorenz96 Pendulum Experiment.

Hyperparameter	cAE	Context-cAE	NcAE
<i>Main Architecture</i>			
Layer Sizes (n_l)	[21, 36]	[20, 36]	[18, 36]
Latent Dimension (d)		2	
Activation parameter α		$\pi/8$	N/A
<i>Contextual Mechanism</i>			
Mechanism	None	Concatenation	Neuromodulation
MLP Topology		N/A	[1, 2, 2, 2]
MLP Activation		N/A	SiLU
Learning rate		N/A	$5 \cdot 10^{-3}$
Weight Decay		N/A	10^{-3}
<i>Optimization</i>			
Optimizer		Riemannian Adam (geoopt)	
Learning Rate		$5 \cdot 10^{-2}$	
Weight Decay		10^{-4}	
Epochs		5000	
Batch Size		512	
Scheduler		ReduceLROnPlateau (Patience 200, Factor 0.9)	